Biosensors and Bioelectronics 261 (2024) 116514

Contents lists available at ScienceDirect

Biosensors and Bioelectronics

journal homepage: www.elsevier.com/locate/bios

A novel low-background nitroreductase fluorescent probe for real-time fluorescence imaging and surgical guidance of thyroid cancer resection

Siqi Zhang [a], Mo Ma [a,b], Chen Zhao [a], Jingkang Li [a], Lanlan Xu [a], Zihe Zhang [c], Quanping Diao [d], Pinyi Ma [a,**], Daqian Song [a,d,*]

[a] College of Chemistry, Jilin Province Research Center for Engineering and Technology of Spectral Analytical Instruments, Jilin University, Qianjin Street 2699, Changchun, 130012, China
[b] School of Pharmacy, Jilin University, Qianjin Street 2699, Changchun, 130012, China
[c] The First Hospital of China Medical University, China Medical University, No. 77 Puhe Road, Shenyang North New Area, Shenyang, 110122, China
[d] Liaoning Key Laboratory of Development and Utilization for Natural Products Active Molecules, School of Chemistry and Life Science, Anshan Normal University, Anshan, China

ARTICLE INFO

Keywords:
Nitroreductase
Low background fluorescence
Thyroid cancer
Fluorescence probe
Imaging *in vivo*

ABSTRACT

Thyroid cancer always appears insidiously with few noticeable clinical symptoms. Due to its limitations, conventional ultrasound imaging can lead to missed or misdiagnosed cases. Surgery is still the primary treatment method of thyroid cancer, but removal of surrounding healthy tissues to minimize recurrence leads to overtreatment and added patient suffering. To address this challenge, herein, a nitroreductase (NTR) fluorescent probe, Ox-NTR, has been developed for detecting thyroid cancer and tracking the surgical removal of thyroid tumors by fluorescence imaging. The conjugated structure of oxazine 1 was disrupted, significantly reducing the issue of high background signals, thus effectively achieving low background fluorescence. Under hypoxic conditions, the nitro group of Ox-NTR can be reduced to an amine and subsequently decomposed into oxazine 1, emitting intense red fluorescence. Ox-NTR has a low detection limit of 0.09 μg/mL for NTR with excellent photostability and selectivity. Cellular studies show that Ox-NTR can effectively detect NTR levels in hypoxic thyroid cancer cells. Moreover, the ability of Ox-NTR of rapid response to thyroid cancer *in vivo* is confirmed by fluorescence imaging in mice, distinguishing tumors from normal tissues due to its superior low background fluorescence. Utilizing this fluorescence imaging method during surgical resection can guide the removal of tumors, preventing both missed tumor tissues and accidental removal of healthy tissue. In summary, the novel Ox-NTR offers precise detection capabilities that provide significant advantages over traditional imaging methods for thyroid cancer diagnosis and treatment, making it a valuable tool to guide tumor removal in surgical procedures.

1. Introduction

Thyroid cancer is the most prevalent malignancy of the head and neck region, representing the most severe form of thyroid disease. It can disrupt endocrine functions, leading to thyroid, pituitary, and adrenal hormone secretion abnormalities (Boucai et al., 2024; Kakudo et al., 2009; Schneider and Chen, 2013). It also has compressive effects on local organs, adversely affecting human health. Papillary thyroid carcinoma, the most common pathological type of thyroid cancer, is insidious without clear clinical symptoms, underscoring the critical importance of monitoring thyroid cancer for overall health (Hwang et al., 2016; La Vecchia et al., 2015). Ultrasonography, a key diagnostic tool for thyroid cancer, may provide non-specific and complex images, making diagnosis challenging and leading to misdiagnosis and missed diagnoses (Hasegawa, 2018; Kumarasinghe and De Silva, 1999; Stasiak et al., 2019; Wu et al., 2017). Therefore, developing a specific diagnostic method to overcome the limitations of common thyroid cancer clinical diagnostic techniques is urgently needed. Currently, the primary treatment for thyroid tumors remains surgical removal (Li, 2018). Moreover, total thyroidectomy is also commonly practiced due to the lack of

* Corresponding author. College of Chemistry, Jilin Province Research Center for Engineering and Technology of Spectral Analytical Instruments, Jilin University, Qianjin Street 2699, Changchun, 130012, China.
** Corresponding author.
E-mail addresses: mapinyi@jlu.edu.cn (P. Ma), songdq@jlu.edu.cn (D. Song).

https://doi.org/10.1016/j.bios.2024.116514
Received 15 May 2024; Received in revised form 17 June 2024; Accepted 19 June 2024
Available online 19 June 2024

effective intraoperative tumor tissue identification technologies. However, a more ideal approach would be near-total thyroidectomy, where only the tumor site is removed while preserving thyroid function. Fluorescence imaging, characterized by its rapidity, non-destructiveness, high sensitivity, high resolution, and low toxicity, emerges as a viable solution to solve these issues (Jin et al., 2018; Li et al., 2023; Qian et al., 2020; Wang and Tang, 2019; Xu et al., 2023). So far, there has been almost no suitable fluorescence probe available for the diagnosis and surgical navigation of thyroid cancer.

Hypoxia is a pervasive phenomenon during the progression of malignant tumors. Therefore, specific hypoxic characteristics of tumors can be utilized to distinguish cancerous from normal tissue (Denny, 2001; Gatenby and Gillies, 2008; McCormack et al., 2013; Semenza, 2012). The hypoxia phenomenon is accompanied by an increase in the expression or over-expression of various related enzymes (de Oliveira et al., 2007; Hecht et al., 1995; Zhang et al., 2019). Nitroreductase (NTR) activity is shown to be positively correlated with the level of hypoxia, typically leading to elevated intracellular NTR levels (Celik and Yetis, 2012; Komatsu et al., 2010; Race et al., 2005). Recent studies have demonstrated that the oxazine 1 fluorescence group can penetrate cells more easily and exhibit higher fluorescence brightness within cells than methylene blue (MB), offering significant advantages (Shang et al., 2022). Most probe molecules are designed based on the intramolecular charge transfer (ICT) principle, which presents inherent disadvantages such as high background fluorescence and poor fluorescence quenching (Ao et al., 2017; Fan et al., 2020; Lin et al., 2022; Liu et al., 2022; Zhai et al., 2017).

In this study, we have developed a fluorescent probe Ox-NTR, specific for NTR, effectively achieving low background fluorescence and significantly resolving the issue of high background fluorescence, to detect thyroid cancer. Moreover, Ox-NTR could be used for fluorescence imaging to monitor the surgical removal of thyroid tumors. Reduced nicotinamide adenine dinucleotide phosphate (NAD(P)H) serves as an electron donor under hypoxic conditions, allowing intracellular NTR to catalyze the single-electron transfer of various exogenous nitroaromatic compounds, forming nitro anion radicals. These substances are further reduced to hydroxylamines or amines, causing the cleavage of the linking groups and subsequently generating oxazine 1, which emits intense fluorescence. Ox-NTR exhibited excellent photostability, and its spectral properties were optimized. Cellular experiments demonstrated that Ox-NTR could effectively detect the expression levels of NTR in hypoxic thyroid cancer cells and validated its specificity towards NTR by introducing inhibitor experiments. The ability of Ox-NTR to detect thyroid cancer *in vivo* was confirmed in mice models using fluorescence imaging. Due to its excellent low background fluorescence advantage, Ox-NTR could rapidly and effectively differentiate between the intensely red fluorescent tumor tissue and the nearly non-fluorescent normal tissue. This stark contrast of fluorescence was further utilized to conduct fluorescence imaging-guided tumor resection, and the tumor tissue was precisely removed along the intense red fluorescence areas. Thus, by combining resection with imaging, we could avoid missing tumor tissues or inadvertently cutting normal tissues until almost no fluorescence signal was detected, indicating complete tumor removal.

2. Experimental procedure

2.1. Probe synthesis

The synthesis process of Ox-NTR is described in Fig. 1.

Ox-NTR. The methodology used to synthesize Ox-NTR was adopted from the previous literature (Shang et al., 2022). Oxazine 1 (700 mg, 0.5 mmol) and sodium carbonate (Na_2CO_3, 212 mg, 2.0 mmol) were dissolved in 7.0 mL of water under a nitrogen atmosphere, and then 6 mL of dichloromethane (CH_2Cl_2) was added. To the above solution, sodium dithionite ($Na_2S_2O_4$, 409 mg, 2.0 mmol) dissolved in 10 mL of water was slowly added, and the reaction mixture was continuously stirred at 40 °C for 1 h until it turned yellow. Subsequently, triethylamine (100 μL, 0.7 mmol) was added dropwise under the nitrogen atmosphere, and the reaction temperature was reduced to below 0 °C. After that, 4-nitrobenzyl chloroformate (108 mg, 0.5 mmol) dissolved in 5 mL of CH_2Cl_2 was added slowly to the above reaction mixture and stirred at 45 °C overnight. Afterward, 20 mL CH_2Cl_2 was added to the reaction mixture under N_2 atmosphere for rapid extraction, and the organic layer was collected. Finally, the solvent was removed via reduced-pressure distillation, and the remaining residue was further purified by silica gel chromatography using petroleum ether and ethyl acetate (v/v, 2:1) as the eluent to obtain the product Ox-NTR as a light blue solid (42.8 mg, yield 16.9%). ^{1}H NMR (600 MHz, DMSO-d_6) δ 8.25 (d, 2H), 7.66 (d, 2H), 7.32 (d, 2H), 6.42 (dd, 2H), 6.35 (d, 2H), 5.35 (s, 2H), 3.32 (s, 8H), 1.08 (t, 12H) (Fig. S1). ^{13}C NMR (151 MHz, DMSO) δ 151.26, 146.64, 137.09, 130.63, 128.85, 125.62, 124.09, 120.39, 106.77, 99.19, 70.25, 44.28, 12.80 (Fig. S2). HR-MS (m/z): Calculated for $[C_{28}H_{32}N_4O_5]^+$: 505.2373, found: 505.2315 (Fig. S3).

2.2. Preparation of samples for spectrophotometric analysis

The 1 mM stock solution of Ox-NTR was prepared in DMSO and stored in a light-protected environment at −40 °C. NTR was dissolved in

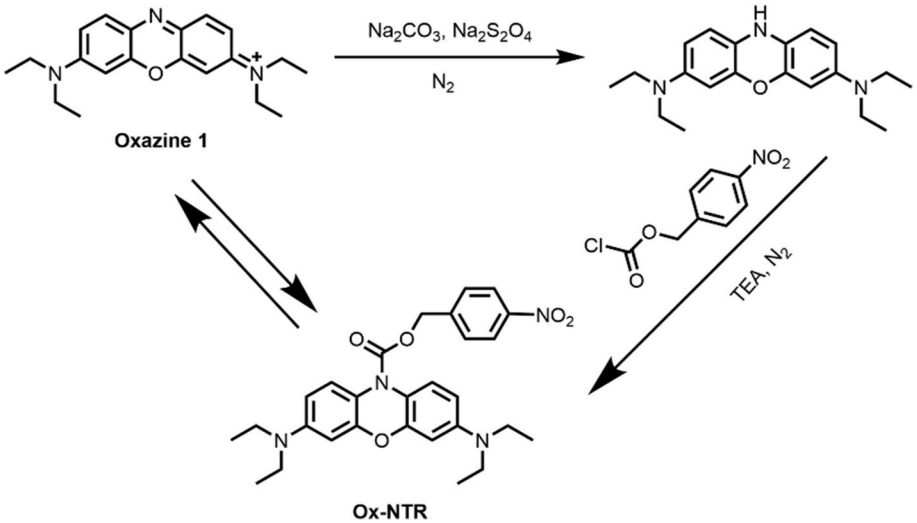

Fig. 1. The synthesis process of Ox-NTR.

sterilized water to a final concentration of 500 μg/mL and then stored in a −80 °C freezer for future use. The Ox-NTR stock solution was re-dissolved in phosphate-buffered saline (PBS, pH = 7.4, 10 mM), and different volumes of NTR solution were added to achieve the desired concentration in the presence of 500 μM (NAD(P)H). The whole volume of PBS, Ox-NTR, NTR, and (NAD(P)H) solutions was maintained at 300 μL. A control solution was prepared without NTR. All samples were then incubated on a 37 °C shaker for 1.5 h before subsequent *in vitro* assays. Finally, the fluorescence emission spectra and UV–vis absorption spectra were obtained at 37 °C using a 1-cm quartz cuvette. The excitation and emission slits widths were set at 10 nm (λ_{ex} = 635 nm, PMT = 700 V).

2.3. Imaging experiment in thyroid cancer model mice

The animal experiment was carried out under the ethical protocols set by Jilin University's Institutional Animal Care and Use Committee (IACUC), certified by the ethical inspection permit number SY202306031.

The TPC-1 cell suspension (containing approximately 1×10^7 cells dissolved in 50 μL of PBS) was subcutaneously injected into the subcutaneous right back of mice, and the tumors were allowed to grow for approximately 2 weeks.

For in situ injection imaging, mice bearing TPC-1 tumors were treated with Ox-NTR (50 μM, 200 μL) by intratumoral injection. Fluorescence imaging was conducted every 20 min post-injection (with the mice being anesthetized with isoflurane). The control group was treated with Ox-NTR injections in an identical manner, and the imaging was performed using a small animal imager.

The tumor-bearing mouse was dissected and peeled after intratumoral injection for fluorescence imaging during fluorescence-mediated surgical resection. Based on the fluorescent images, the tumor was surgically resected, and the mouse was re-imaged. Main organs (heart, liver, spleen, lung, and kidney) and TPC-1 tumor were collected for further fluorescent imaging.

3. Results and discussion

3.1. Molecular design of Ox-NTR

Although MB is widely used in fluorescence imaging due to its ease of entry into cells, its practical application is hindered due to the requirement of an excitation laser to generate singlet oxygen, low quantum yield, and its potential toxicity. To overcome these challenges, we have employed the oxazine 1 fluorophore, known for its high fluorescence brightness within cells, hence offering a better alternative due to its excellent cell permeability and brightness. Most organic fluorescent probes for NTR always rely on the ICT mechanism for their fluorescence quenching due to the strong electron-withdrawing capability of nitro groups. However, this quenching is always incomplete, leading to high background fluorescence, which could compromise imaging performance. In our approach, we utilize oxazine 1 as the fluorophore and disrupt its rigid conjugated structure by adding $Na_2S_2O_4$. This disruption theoretically leads to fluorescence quenching without the need for additional molecular mechanisms, as confirmed in subsequent *in vitro* experiments. As stated earlier, nitro groups are commonly used as receptor units in NTR fluorescent probes. Instead of merely linking the nitro group directly to the fluorophore, in our design, a linker structure nitrobenzyl alcohol is introduced into the oxazine 1. Upon reaction with NTR, the nitro group converts into an amine, forming an amine-benzyl alcohol, a typical self-eliminating linker in Ox-NTR structure. This flexible linker allows a complete interaction of the molecular recognition site of Ox-NTR with the active site of NTR, promoting a comprehensive reaction with NTR. This design keeps the enzyme recognition site adequately separated from the hydrophobic fluorophore, enhancing chemical stability and enzymatic reactivity, and provides a potent tool for the specific detection of NTR, which is crucial for fluorescent imaging and biological applications. Fig. S4 illustrates the potential reaction mechanism of Ox-NTR with NTR. Thus, functionalization of the oxazine 1 fluorophore results in an exceptional low-background fluorescent probe Ox-NTR that enhances the capabilities of fluorescence imaging and expands its biological applications.

3.2. Spectral characterization of Ox-NTR before and after reaction with NTR

The probe Ox-NTR displayed a very low-intensity UV–vis absorption at 635 nm. As shown in Fig. 2A, the intensity of the 635 nm peak significantly increased upon the addition of enough (NAD(P)H) and NTR (20 μg/mL). Concomitantly, the color of the solution also changed from nearly colorless to light blue, further confirming the transformation of Ox-NTR into oxazine 1 upon interaction with NTR. Next, we explored the change in the fluorescence spectrum of Ox-NTR upon adding NTR. The fluorescence intensity of the system was immediately recorded every 10 min after the addition of NTR to explore the optimal reaction time for subsequent *in vitro* experiments (Fig. S5). As evidenced in Fig. 2B, there was a notable increase in fluorescence intensity at 683 nm after the addition of NTR (20 μg/mL) upon using 635 nm as the excitation wavelength. Next, NTR solutions of different concentrations ranging from 0 to 20 μg/mL were added to the reaction system, and fluorescence emission intensities at 683 nm were measured (Fig. 2C). The fluorescence intensity increased progressively with the increased NTR concentration, reaching a maximum of 13.3 times the fluorescence intensity without NTR. Furthermore, the LOD of Ox-NTR, calculated using the 3σ/k formula, was as low as 0.09 μg/mL. The fluorescence emission intensity at 683 nm demonstrated a strong linear relationship with the concentration of NTR in the 0–2.0 μg/mL range, with a correlation coefficient R = 0.991 (Fig. 2D). The strong linear response suggested the potential of Ox-NTR for accurate NTR quantification in various samples.

3.3. Optimization of reaction conditions

To optimize the reaction conditions between the probe Ox-NTR and NTR, the stability of Ox-NTR, oxazine 1, and the reaction solution were evaluated under laser irradiation with a 635 nm excitation laser for 1 h. As illustrated in Fig. S6, the fluorescence intensity of Ox-NTR, oxazine 1, and the reaction system remained almost stable, indicating good photostability of Ox-NTR, which is suitable for long-term applications in biological imaging.

Next, the effects of temperature and pH on the reaction system were explored. Minimal variation in fluorescence intensity of the reaction system was observed across different pH levels (pH = 4, 5, 6, 7.4, 8, 9). Even though the fluorescence intensity did not maximize at pH = 7.4, it still confirmed the good interaction between Ox-NTR and NTR. Given that the optimal physiological pH in biological systems is 7.4, this pH level was selected as the optimal for the subsequent experiments. Furthermore, the effect of different temperatures (25, 30, 37, and 42 °C) on the fluorescence of the reaction system was investigated. The fluorescence intensity at 37 °C demonstrated effective binding between Ox-NTR and NTR, matching the internal temperature of biological organisms. Therefore, 37 °C was chosen as the optimal temperature for the subsequent experiments (Fig. S8). These optimized conditions ensured the effective function of Ox-NTR within typical biological environments, enhancing its applicability for NTR detection in bioimaging applications.

3.4. Selectivity of the probe Ox-NTR for NTR

The specificity of the probe Ox-NTR for NTR was further investigated to ascertain its specific recognition ability. The response of Ox-NTR was tested for 49 common biological substances, including cations, anions, amino acids, and enzymes in cells. The fluorescence emission intensity

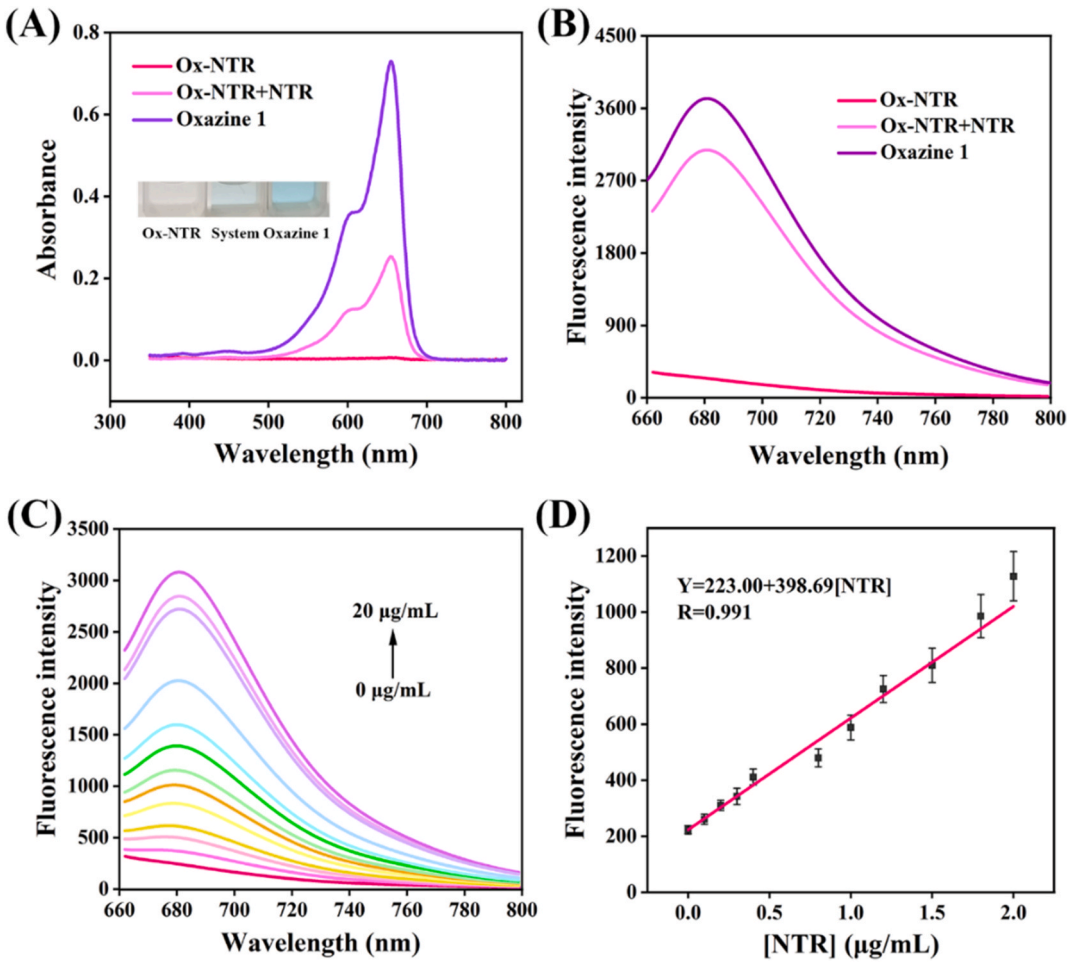

Fig. 2. (A) UV–vis absorption spectra of Ox-NTR (10 μM), reaction system (Ox-NTR + NTR), and oxazine 1 (10 μM). (B) Fluorescence spectra of Ox-NTR (10 μM), reaction system, and oxazine 1 (10 μM), λ_{ex} = 635 nm. (C) Fluorescence spectra of Ox-NTR following the gradual addition of NTR, λ_{ex} = 635 nm. (D) Linear relationship between fluorescence intensity (I_{683}) of Ox-NTR and NTR concentrations (0–2 μg/mL), λ_{ex} = 635 nm.

of Ox-NTR at 683 nm was measured in the presence of the above-interfering substances. No significant changes in the 683 nm fluorescence emission intensity were observed, demonstrating a negligible response of Ox-NTR to these common biological substances compared to its response to NTR. The results confirmed that Ox-NTR could specifically detect NTR without interference from other common biological substances (Fig. S9). Moreover, coumarin (0.5 mM), a known inhibitor of NTR, was added to the system to assess Ox-NTR specificity for NTR. The presence of the excess inhibitor led to a decrease in the fluorescence intensity of the system, indicating the binding of Ox-NTR with NTR, further validating the specificity of Ox-NTR for NTR (Fig. S10). These results conclusively demonstrated the specific binding of Ox-NTR to NTR, laying a solid foundation for subsequent biological detection and applications.

3.5. Molecular docking of Ox-NTR with NTR

Molecular docking experiments were also conducted to simulate the binding interaction between Ox-NTR and NTR. As observable in Fig. 3, Ox-NTR easily penetrated the active site of NTR and bound to it. NTR subsequently cleaved the recognition site of Ox-NTR, resulting in the release of Oxazine 1 and an increase in fluorescence signal. The binding energy was calculated to be −9.4 kcal/mol. Ox-NTR also formed two hydrogen bonds with two amino acids of NTR (ASN117 and ARG207).

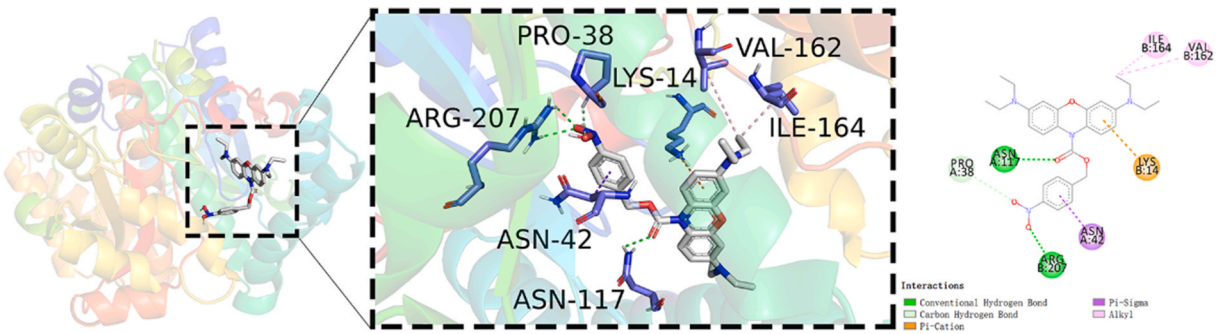

Fig. 3. Simulation of interactions between Ox-NTR and NTR.

These results demonstrate the effective binding of the probe Ox-NTR with NTR.

3.6. Cytotoxicity experiments

The cytotoxicity of the probe Ox-NTR was assessed using the CCK-8 assay to determine its potential adverse effects on the health of cells, specifically targeting thyroid cancer cells (TPC-1). This evaluation aimed to confirm the feasibility of using Ox-NTR in subsequent cellular experiments. As evidenced in Fig. S11, the cell viability remained above 85% after incubating TPC-1 cells with various concentrations of Ox-NTR for 24 h. The high cell viability indicated the low cytotoxicity of Ox-NTR towards TPC-1 cells, which was a crucial prerequisite for its use in cellular experiments. This result ensured that Ox-NTR could be safely used for further biological assessments without harming the cellular integrity.

3.7. Hypoxic experiments using Ox-NTR for imaging

Extensive literature indicates that the hypoxic environment within tumor cells can lead to an increase in intracellular NTR (Bader et al., 2021; Konisti et al., 2012; Li et al., 2015; Nejad et al., 2021; Zhou et al., 2021). To investigate NTR expression in hypoxic TPC-1 cells, a tri-gas incubator was used to simulate the hypoxic environment of the tumor and investigate NTR expression in hypoxic TPC-1 cells, and the results were compared with normoxic cells. After adding Ox-NTR, cellular imaging was performed at different time points under normal oxygen (20% O_2) and hypoxic environment (5% O_2). As displayed in Fig. 4, the fluorescence intensity in TPC-1 cells was notably low under normoxic conditions at the 60-min point, whereas fluorescence signals increased markedly in TPC-1 cells under hypoxic conditions. This outcome suggested that after 60 min of incubation under hypoxia, cells produced significant amounts of NTR, which later bound to Ox-NTR. Contrarily, normoxic cells did not produce as much NTR, leading to a lower

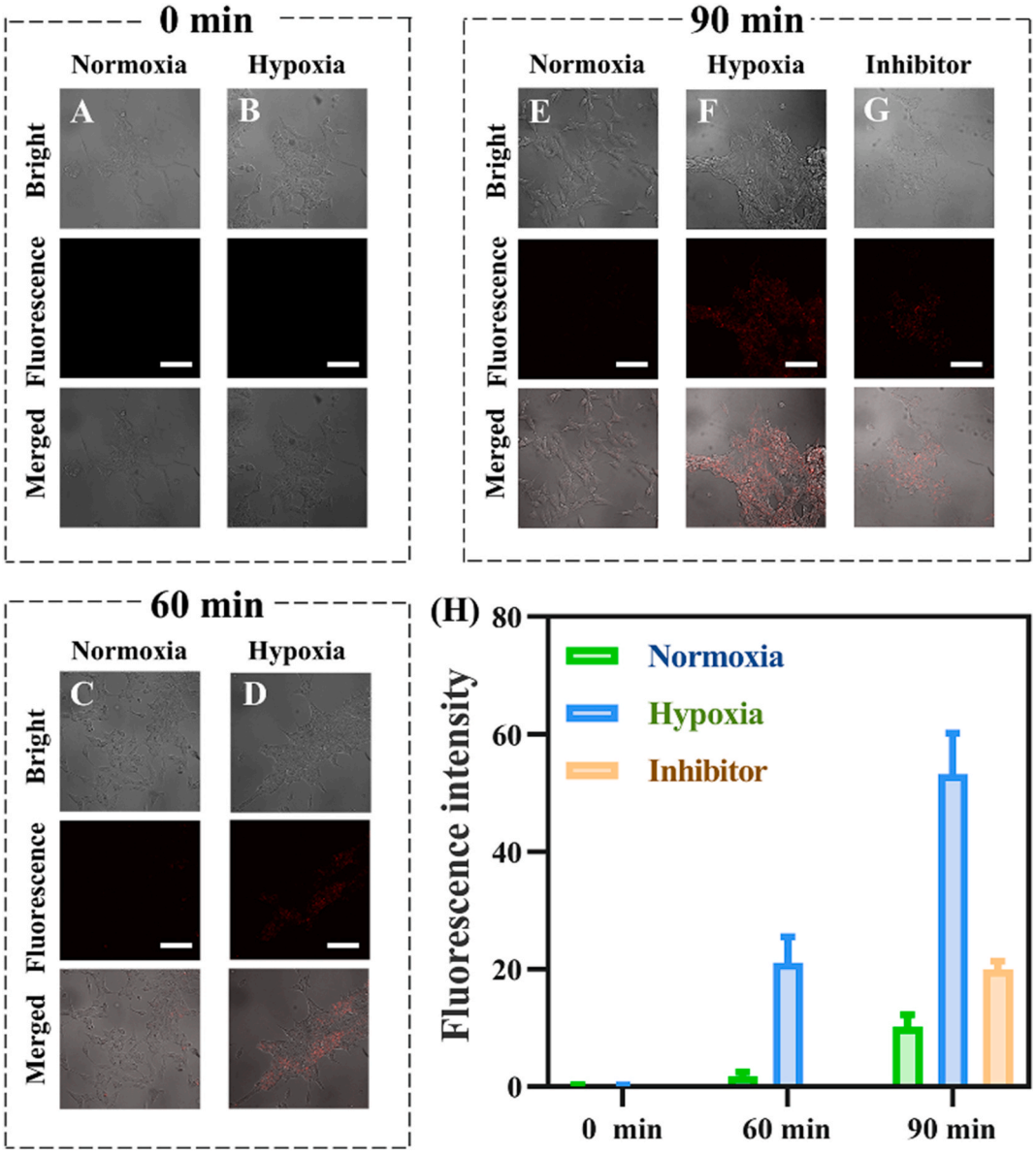

Fig. 4. Fluorescence imaging of TPC-1 cells after incubation with 10 μM Ox-NTR for (A) 0 min in normoxia, (B) 0 min in hypoxia, (C) 60 min in normoxia, (D) 60 min in hypoxia, (E) 90 min in normoxia, (F) 90 min in hypoxia. (G) Hypoxia TPC-1 cells were pretreated with 10 mM coumarin for 1 h and then incubated with 10 μM Ox-NTR for 90 min. (H) Comparison of the fluorescence intensities obtained under the conditions above-mentioned. λ_{ex} = 605–640 nm, λ_{em} = 670–715 nm. Scale bar, 100 μm.

fluorescence intensity. This experiment confirmed a substantial increase in NTR levels in hypoxic TPC-1 cells, and the upregulation of tumor markers was detectable using the probe Ox-NTR. At the 90-min time point, the fluorescence intensity in hypoxic cells was much higher than in both normoxic cells and the 60-min hypoxic cells, implying that hypoxic cells not only produce more NTR than normoxic cells but also continuously react with Ox-NTR to form the oxazine 1 fluorophore with the prolongation of incubation time of Ox-NTR, resulting in increased fluorescence intensity (Fig. 4). The above results demonstrated that NTR could serve as a thyroid cancer indicator, which could be detected through fluorescence imaging using Ox-NTR. Furthermore, the specificity of Ox-NTR for NTR at the cellular level was confirmed by pretreating TPC-1 cells with 10 mM coumarin (an NTR inhibitor) before imaging. As evident from Fig. 4, the fluorescence intensity significantly decreased in the inhibitor-treated group, indicating that the intracellular fluorescence change was specifically due to the endogenous cleavage of Ox-NTR by NTR and the subsequent release of the oxazine 1 fluorophore. This finding further verified the specific recognition capability of Ox-NTR for NTR in a cellular environment.

3.8. *In vivo* imaging and surgically induced tumor resection

The previous results of this study established the spectral characteristics of Ox-NTR and demonstrated its application for NTR detection in cellular experiments. Due to its low background fluorescence, Ox-NTR proved a valuable tool for *in vivo* imaging. To further explore the potential of Ox-NTR in detecting thyroid cancer *in vivo*, thyroid cancer mice models were constructed. To the best of our knowledge, this is the first NTR probe used in the specific organ of the thyroid gland, representing a novel exploration.

Since the intratumoral injection is straightforward and offers a high targeting efficiency and rapid response, 200 μL of Ox-NTR (50 μM) was directly injected into the tumor site, while the same concentration and volume were injected into the corresponding site in healthy mice as control. As shown in Fig. S12, the fluorescence intensity between tumor-bearing and healthy mice was markedly different at 10 min. Such a fast response time had a huge advantage over the molecules reported in the literature (Table S1). This indicated that Ox-NTR had a fast reaction time in the organism, and could be used in real-time monitoring in the organism. However, tumor-bearing mice exhibited much higher fluorescence intensity than healthy mice over time, and the difference became more pronounce. This observation suggested that significant amounts of NTR were produced in the hypoxic tumor sites of cancerous mice, reacting with Ox-NTR to release the oxazine 1 fluorophore and emitting a strong red fluorescence signal. In contrast, healthy mice did not produce comparable amounts of NTR. These findings align with the cell experiments and underscore the effectiveness of Ox-NTR as a diagnostic tool for thyroid cancer. Based on these results and the ability of Ox-NTR to distinguish tumor sites (strong red fluorescence) and normal sites (almost no fluorescence), the potential of Ox-NTR to guide tumor resection was hypothesized. The skin over the tumor site on the right back of the mice was peeled for imaging after 2 h of Ox-NTR injection, revealing a prominent fluorescence signal (Fig. 5A). The tumor was then excised along the red fluorescence area while imaging, ensuring no tumor tissue was missed, and almost no normal tissue was mistakenly excised. Once only normal tissue with almost no fluorescence signal remained, the tumor was deemed completely removed (Fig. 5B and C). Finally, the tumor-bearing mice were dissected for fluorescence imaging of the primary organs—heart, liver, spleen, lung, kidney, and tumor tissues. As evidenced in Fig. 5D, fluorescence signals from the heart, liver, spleen, lung, and kidney were negligible compared to the strong red fluorescence of the tumors, indicating that the hypoxic tumor site produced more NTR, reacting with Ox-NTR to distinguish thyroid cancer tumors from normal tissues.

Overall, these findings suggest that Ox-NTR is an effective imaging agent for detecting thyroid cancer and can prove a valuable tool for assisting in the fluorescence-guided surgical resection of tumors, significantly enhancing surgical outcomes by enabling more precise tumor removal while minimizing damage to surrounding healthy tissues.

4. Conclusions

In summary, a novel near-infrared probe, Ox-NTR, was successfully

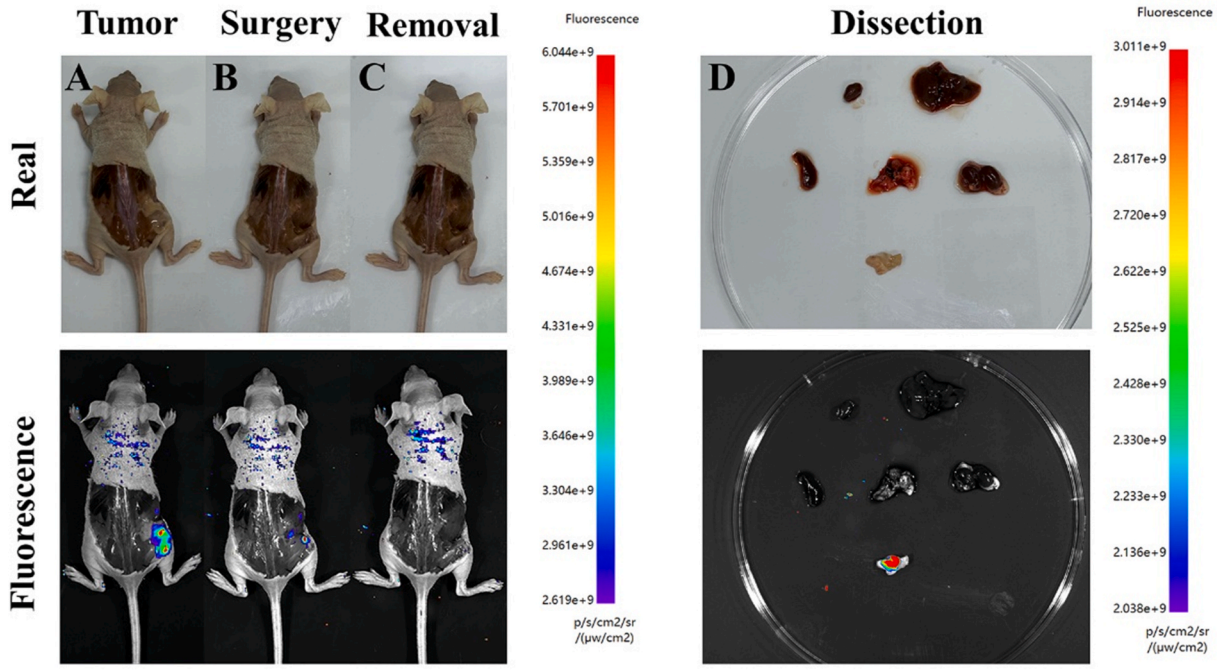

Fig. 5. (A) Images of TPC-1 tumor-bearing mouse. (B) Imaging-guided resection of the tumor in situ. (C) Images of tumor removal. (D) Images of the main internal organs and TPC-1 tumor.

designed with superior specificity for NTR detection. The effective quenching of fluorescence was realized by Ox-NTR. Ox-NTR demonstrated excellent photostability, with a fluorescence enhancement of 13 times upon interaction with NTR. However, the Stokes shift of Ox-NTR showed short. Based on this, we would improve this issue to magnify the Stokes shift in the future work. Ox-NTR showed high biocompatibility and specificity for NTR. At the cellular level, Ox-NTR proved a valuable tool for screening thyroid cancer. Furthermore, *in vivo* imaging results in mice confirmed its ability to distinguish thyroid tumors from normal tissues rapidly. The probe successfully guided surgical resection of thyroid tumors through fluorescence imaging, achieving near-total thyroidectomy. In conclusion, the accurate detection capabilities of the novel Ox-NTR fluorescent probe offer substantial advantages over traditional imaging methods and provide a valuable tool for the surgical removal of tumor tissue in future.

CRediT authorship contribution statement

Siqi Zhang: Writing – original draft, Validation, Investigation, Data curation, Conceptualization. **Mo Ma:** Methodology, Investigation, Data curation. **Chen Zhao:** Investigation, Data curation. **Jingkang Li:** Investigation, Data curation. **Lanlan Xu:** Investigation, Data curation. **Zihe Zhang:** Software, Formal analysis. **Quanping Diao:** Software, Formal analysis. **Pinyi Ma:** Writing – review & editing, Software, Project administration, Data curation, Conceptualization. **Daqian Song:** Supervision, Resources, Project administration, Funding acquisition.

Declaration of competing interest

The authors declare that they have no known competing financial interests or personal relationships that could have appeared to influence the work reported in this paper.

Data availability

Data will be made available on request.

Acknowledgement

This work was supported by the National Natural Science Foundation of China (22004046 and 22074052) and the Science and Technology Developing Foundation of Jilin Province of China (Nos. 20230101033JC and 20240404044ZP).

Appendix A. Supplementary data

Supplementary data to this article can be found online at https://doi.org/10.1016/j.bios.2024.116514.

References

Ao, X., Bright, S.A., Taylor, N.C., Elmes, R.B.P., 2017. Org. Biomol. Chem. 15 (29), 6104–6108.
Bader, S.B., Dewhirst, M.W., Hammond, E.M., 2021. Cancers 13 (1), 23.
Boucai, L., Zafereo, M., Cabanillas, M.E., 2024. Jama-j. Am. Med. Assoc. 331 (5), 425–435.
Celik, A., Yetis, G., 2012. Bioorgan. Med. Chem. 20 (11), 3540–3550.
de Oliveira, I.M., Pegas Henriques, J.A., Bonatto, D., 2007. Biochem. Bioph. Res. Co 355 (4), 919–925.
Denny, W.A., 2001. Eur. J. Med. Chem. 36 (7–8), 577–595.
Fan, L., Zan, Q., Lin, B., Wang, X., Gong, X., Zhao, Z., Shuang, S., Dong, C., Wong, M.S., 2020. Analyst 145 (16), 5657–5663.
Gatenby, R.A., Gillies, R.J., 2008. Nat. Rev. Cancer 8 (1), 56–61.
Hasegawa, H., 2018. J. Med. Ultrason. 45 (1), 1, 1.
Hecht, H.J., Erdmann, H., Park, H.J., Sprinzl, M., Schmid, R.D., 1995. Nat. Struct. Biol. 2 (12), 1109–1114.
Hwang, S.H., Kim, E.-K., Moon, H.J., Yoon, J.H., Kwak, J.Y., 2016. Korean. J. Radiol. 17 (2), 255–263.
Jin, X., Wu, X., Xie, P., Liu, S., Wu, J., Wang, T., Zhou, H., Leng, X., Chen, W., 2018. Anal. Methods 10 (33), 4079–4084.
Kakudo, K., Bai, Y., Katayama, S., Hirokawa, M., Ito, Y., Miyauchi, A., Kuma, K., 2009. Pathol. Int. 59 (6), 359–367.
Komatsu, H., Harada, H., Tanabe, K., Hiraoka, M., Nishimoto, S.-i., 2010. Medchemcomm 1 (1), 50–53.
Konisti, S., Kiriakidis, S., Paleolog, E.M., 2012. Nat. Rev. Rheumatol. 8 (3), 153–162.
Kumarasinghe, M.P., De Silva, S., 1999. Pathology 31 (1), 1–7.
La Vecchia, C., Malvezzi, M., Bosetti, C., Garavello, W., Bertuccio, P., Levi, F., Negri, E., 2015. Int. J. Cancer 136 (9), 2187–2195.
Li, J., Cao, J., Wu, W., Xu, L., Zhang, S., Ma, P., Wu, Q., Song, D., 2023. Sensor Actuat. B-chem 377, 133122.
Li, K., 2018. Pediatric Blood & Cancer, 65, p. S479. S479.
Li, Y., Sun, Y., Li, J., Su, Q., Yuan, W., Dai, Y., Han, C., Wang, Q., Feng, W., Li, F., 2015. J. Am. Chem. Soc. 137 (19), 6407–6416.
Lin, Q., Li, C., Wang, L., Cai, H., Tang, L., Gu, Y., 2022. Sensor Actuat. B-chem 371, 132521.
Liu, X., Zeng, S., Zhang, M., Jiang, M., Kafuti, Y.S., Shangguan, P., Yu, Y., Chen, Q., Wang, J., Peng, X., Yoon, J., Li, H., 2022. Chem. Commun. 58 (81), 11438–11441.
McCormack, E., Silden, E., West, R.M., Pavlin, T., Micklem, D.R., Lorens, J.B., Haug, B.E., Cooper, M.E., Gjertsen, B.T., 2013. Cancer Res. 73 (4), 1276–1286.
Nejad, A.E., Najafgholian, S., Rostami, A., Sistani, A., Shojaeifar, S., Esparvarinha, M., Nedaeinia, R., Javanmard, S.H., Taherian, M., Ahmadlou, M., Salehi, R., Sadeghi, B., Manian, M., 2021. Cancer Cell Int. 21 (1), 62.
Qian, J., Teng, Z., Wang, J., Zhang, L., Cao, T., Zheng, L., Cao, Y., Qin, W., Liu, Y., Guo, H., 2020. ACS Sens. 5 (9), 2806–2813.
Race, P.R., Lovering, A.L., Green, R.M., Ossor, A., White, S.A., Searle, P.F., Wrighton, C. J., Hyde, E.I., 2005. J. Biol. Chem. 280 (14), 13256–13264.
Schneider, D.F., Chen, H., 2013. Ca-cancer. J. Clin. 63 (6), 373–394.
Semenza, G.L., 2012. Cell 148 (3), 399–408.
Shang, J., Zhang, X., He, Z., Shen, S., Liu, D., Shi, W., Ma, H., 2022. Angew. Chem. Int. Ed. Engl. 61 (33), e202205043.
Stasiak, M., Michalak, R., Lewinski, A., 2019. BMC Endocr. Disord 19 (1), 86.
Wang, D., Tang, B.Z., 2019. Accounts Chem. Res. 52 (9), 2559–2570.
Wu, Z.G., Yan, X.Q., Su, R.S., Ma, Z.S., Xie, B.J., Cao, F.L., 2017. World J. Surg. 41 (1), 129–135.
Xu, L., Chu, H., Gao, D., Wu, Q., Sun, Y., Wang, Z., Ma, P., Song, D., 2023. Anal. Chem. 95, 2949–2957.
Zhai, B., Hu, W., Sun, J., Chi, S., Lei, Y., Zhang, F., Zhong, C., Liu, Z., 2017. Analyst 142 (9), 1545–1553.
Zhang, J., Chai, X., He, X.-P., Kim, H.-J., Yoon, J., Tian, H., 2019. Chem. Soc. Rev. 48 (2), 683–722.
Zhou, H., Guo, M., Li, J., Qin, F., Wang, Y., Liu, T., Liu, J., Sabet, Z.F., Wang, Y., Liu, Y., Huo, Q., Chen, C., 2021. J. Am. Chem. Soc. 143 (4), 1846–1853.